Step-on versus step-off signals in time-domain controlled source electromagnetic methods using a grounded electric dipole

Amir Haroon[1]*, Andrei Swidinsky[2], Sebastian Hölz[1], Marion Jegen[1] and Bülent Tezkan[3]

[1] *Research Department 4 - Dynamics of the Ocean Floor, Helmholtz Centre for Ocean Research, GEOMAR, Kiel, Wischhofstr. 1-3, Kiel, 24148, Germany,* [2] *Department of Geophysics, Colorado School of Mines, Golden, CO 80401, USA, and* [3] *Department of Geoscience, Institute of Geophysics and Meteorology, University of Cologne, Cologne, 50963, Germany*

ABSTRACT

The time-domain controlled source electromagnetic method is a geophysical prospecting tool applied to image the subsurface resistivity distribution on land and in the marine environment. In its most general set-up, a square-wave current is fed into a grounded horizontal electric dipole, and several electric and magnetic field receivers at defined offsets to the imposed current measure the electromagnetic response of the Earth. In the marine environment, the application often uses only inline electric field receivers that, for a 50% duty-cycle current waveform, include both step-on and step-off signals. Here, forward and inverse 1D modelling is used to demonstrate limited sensitivity towards shallow resistive layers in the step-off electric field when transmitter and receivers are surrounded by conductive seawater. This observation is explained by a masking effect of the direct current signal that flows through the seawater and primarily affects step-off data. During a step-off measurement, this direct current is orders of magnitude larger than the inductive response at early and intermediate times, limiting the step-off sensitivity towards shallow resistive layers in the seafloor. Step-on data measure the resistive layer at times preceding the arrival of the direct current signal leading to higher sensitivity compared to step-off data. Such dichotomous behaviour between step-on and step-off data is less obvious in onshore experiments due to the lack of a strong overlying conductive zone and corresponding masking effect from direct current flow. Supported by synthetic 1D inversion studies, we conclude that time-domain controlled source electromagnetic measurements on land should apply both step-on and step-off data in a combined inversion approach to maximize signal-to-noise ratios and utilize the sensitivity characteristics of each signal. In an isotropic marine environment, step-off electric fields have inferior sensitivity towards shallow resistive layers compared to step-on data, resulting in an increase of non-uniqueness when interpreting step-off data in a single or combined inversion.

Key words: Electromagnetics, Modelling, Noise, Numerical study, Resistivity.

INTRODUCTION

Controlled source electromagnetic (CSEM) methods are used on land and in the marine environment to image the subsurface resistivity distribution. Common applications include, but are not limited to hydrocarbon and geothermal exploration

*E-mail: aharoon@geomar.de

(e.g. Kaufman and Keller, 1983; Keller *et al.*, 1984; Constable, 2010), gas hydrate and methane seep detection (e.g. Weitemeyer *et al.*, 2011; Gehrmann *et al.*, 2016; Goswami *et al.*, 2016; Schwalenberg *et al.*, 2017; Attias *et al.*, 2018), mineral exploration (e.g. Gehrmann *et al.*, 2019; Mörbe *et al.*, 2020) and environmental research such as mud volcano imaging (e.g. Haroon *et al.*, 2015; Hölz *et al.*, 2015) or offshore groundwater studies (e.g. Haroon *et al.*, 2018b; Levi *et al.*, 2018; Micallef *et al.*, 2018; Gustafson *et al.*, 2019; Lippert and Tezkan, 2020). In a CSEM survey, current is injected into the subsurface via a grounded horizontal electrical dipole (HED) antenna, and the response of the Earth is measured by one or more electric and/or magnetic field receivers located at various distances from the source. The received signal is a function of the input current, which is modified by the resistivity structure of the Earth between the transmitter and receiver, by the acquisition system itself; superimposed on this response are various sources of anthropogenic and natural noise (Strack, 1992).

CSEM applications are commonly conducted in either the time or the frequency domain. In a time-domain CSEM (TD-CSEM) experiment, a square-wave current with either a 50% (e.g. Cairns, 1997; Yuan and Edwards, 2000) or 100% duty cycle (e.g. Hördt *et al.*, 1992; Schwalenberg *et al.*, 2005) is commonly used. These current waveforms differ in the way that the amplitude switches from one polarity to the other, which occurs rapidly in a 100% duty cycle and is interrupted by a zero state in the 50% duty-cycle signal. Hence, the measured electric field contains both step-on and step-off signals when transmitting a 50% duty cycle and polarity reversals (negative to positive current switch or *vice versa*) in a 100% duty cycle.

For marine frequency-domain CSEM (FD-CSEM), the 100% duty-cycle current waveform is typically used and has been effectively applied in numerous academic and industrial surveys (Myer *et al.*, 2011). Particularly in marine electromagnetic surveys targeting hydrocarbons, FD-CSEM is the method of choice due to its high efficiency. Yet, until very recently it was believed that seafloor-based FD-CSEM receivers lose sensitivity when applied in environments with limited water depth above the source and receivers (<300 m; e.g. Weiss, 2007) due to a masking effect of the air–sea interface, sometimes referred to as the airwave (Weidelt, 2007). However, Chave *et al.* (2017a, 2017b) have recently demonstrated using forward modelling that submerged FD-CSEM systems are effective in shallow marine environments. Alternatively, surface-towed FD-CSEM systems are often applied to mitigate the effect of the air–sea interface (e.g. Sherman *et al.*, 2017; Sherman

and Constable, 2018; Gustafson *et al.*, 2019). However, surface-towed CSEM suffers from a decrease in sensitivity due to signal attenuation in the conductive seawater and is mostly applied along continental shelves with limited water column thicknesses (e.g. Sherman *et al.*, 2017; Gustafson *et al.*, 2019).

To increase seafloor coupling and reduce the airwave signal contribution, academic CSEM surveys targeting shallow resistive structures (depth below seafloor ≤100 m) sometimes apply seafloor-towed TD-CSEM using either a 100% (e.g. Schwalenberg *et al.*, 2017) or a 50% duty-cycle signal (e.g. Yuan and Edwards, 2000). These seafloor-based TD-CSEM applications generally have high sensitivity for sub-seafloor resistivity structures but are less efficient (compared to FD-CSEM) in terms of survey speed (only survey at an average speed of approximately 1 kn), and longer acquisition windows are needed to reach the direct current (DC) state. Here, we demonstrate that TD-CSEM applications show dissimilar behaviour between step-on and step-off data. A short comparison to FD-CSEM systems in an equivalent transmitter–receiver set-up indicates that signal amplitudes acquired in the frequency domain behave similar to step-on data (Appendix A1). However, we note that the comparison between FD-CSEM and TD-CSEM is included here only for completeness but should not be over-interpreted due to the reasons explained in Appendix A1. For an in-depth comparison between TD-CSEM and FD-CSEM, we refer to, for example Andreis and MacGregor (2007), Connell (2011), Connell and Key (2013), and Mörbe (2020).

TD-CSEM applications often apply a 50% duty-cycle current to make use of the superior ramp characteristics in the switch-off step (e.g. Lippert and Tezkan, 2020; Micallef *et al.*, 2020). Non-linear signal distortions such as overshoots, spikes and drifts are commonly less pronounced in the step-off current making them favourable for interpretation. However, we demonstrate here that restricting the interpretation to step-off data affects not only signal-to-noise considerations, but also limits the sensitivity of the TD-CSEM method to resolve shallow resistive structures in the seafloor. This is not a statistical consequence but originates instead from the physical differences between the step-on and the step-off electric fields.

For land-based TD-CSEM acquisition, Kaufman and Keller (1983, p. 385) discuss fundamental physical differences between step-on and step-off electric fields. They illustrate that step-on and frequency-domain soundings are screened by a layer of infinite resistivity in the subsurface, whereas step-off signals become practically horizontal and do not create charges on the surfaces of the resistive layer. Hence, step-off signals can detect layers located at greater depth than the
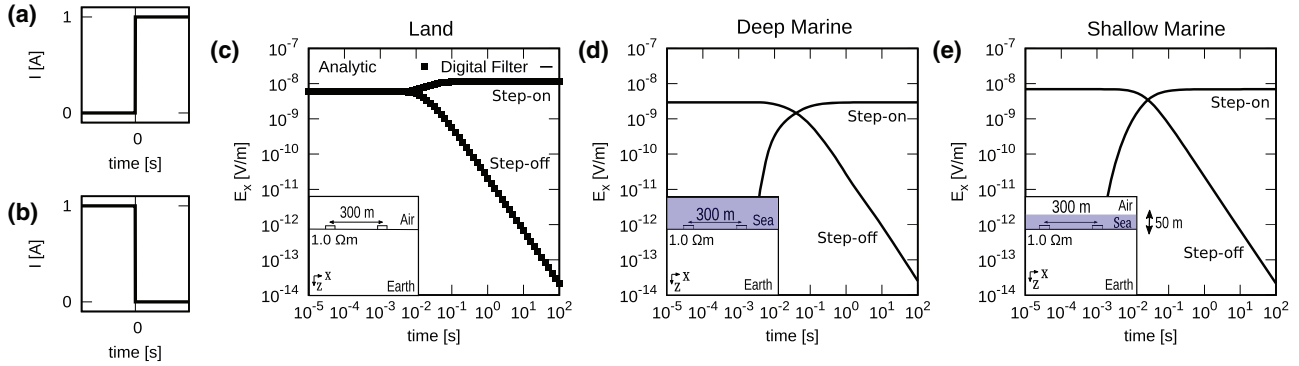
Figure 1 (a) Step-on and (b) step-off current functions for 1 A current. (c) Land-based TD-CSEM signals and benchmark test between the analytic (square markers) and Hankel–Laplace solution (digital filter) for a surface-based horizontal electrical dipole transmitter and an inline electric field receiver at an offset of 300 m. (d) Hankel–Laplace transform solution for an inline transmitter–receiver system sitting on the interface between an infinitely thick seawater layer of 0.33 Ωm and a 1 Ωm seafloor. (e) Hankel–Laplace solution for an inline transmitter–receiver system sitting on the interface of a shallow seawater layer of 0.33 Ωm and 50 m thickness and a 1 Ωm seafloor. Simulations are conducted for a point-dipole source and receiver.

resistive layer, whereas step-on signals cannot. These fundamental differences between step-on and step-off electric fields are often neglected, since the common opinion is that both current excitations are equivalent in terms of sensitivity. This paper reiterates sensitivity characteristics of step-on and step-off electric fields on land and translates them to the deep marine (infinite water depth) and shallow marine (50 m water depth) environments, where differences in sensitivity are even more severe. It should be noted that multiple definitions of shallow marine environment exist (e.g. Weiss, 2007; Sommer *et al.*, 2013). We constrain water column thickness for the shallow marine models to 50 m, which satisfies the conditions of both above-mentioned publications.

Haroon (2016) shows that the detectability of a shallow 1D marine resistor (i.e. applicable to offshore groundwater or gas hydrate investigations) is orders of magnitude larger when measuring the electric field from a step-on signal compared to signals from a step-off current step. Although he uses this observation to design a TD-CSEM system for offshore groundwater exploration, no explanation is given regarding the physical principles that dictate the sensitivity differences between step-on and step-off data. Here, we use 1D modelling to demonstrate these sensitivity differences and describe the physical processes that lead to this dichotomous behaviour between the two signals in a marine setting. Different noise considerations are used to illustrate the relationship between sensitivity and data errors before implications of using either step-on or step-off data (or a combination of both) are investigated using 1D inversion.

METHODOLOGY

To derive the relationship between step-on and step-off electric fields of an horizontal electrical dipole (HED) source, let us first consider an external current step function $I^e(t)$ that at $t = 0$ seconds is instantaneously turned on (Fig. 1a). Hence,

$$I^e(t) = |I| \times \Theta(t),\tag{1}$$

where $\Theta(t)$ is the Heaviside function that equals unity for $t > 0$ seconds and zero for $t < 0$ seconds. $|I|$ is the amplitude of the imposed external current oriented in a certain direction in space. Following Ward and Hohmann (1988), the step-response $f(t)$ is given by the integral of the impulse $h(t)$ that for a causal system is defined as

$$f(t) = \int_0^t h(\tau)\, d\tau \quad t \geq 0.\tag{2}$$

When measuring the decay of the field after a constant current is turned off, that is, a negative step $I^e(-t) = 1 - I^e(t)$ displayed in Fig. 1(b), the step-off function $f^-(t)$ is written as

$$f^-(t) = \int_t^\infty h(\tau)\, d\tau = \int_0^\infty h(\tau)\, d\tau - \int_0^t h(\tau)\, d\tau \quad t \geq 0\tag{3}$$

or

$$f^-(t) = f(\infty) - f(t) \quad t \geq 0,\tag{4}$$

where the integral of h from 0 to ∞ is the direct current (DC) response. We apply (4) to calculate the electric field of an HED after a constant current is shut off:

$$E_{\text{off}}(t) = E_{\text{DC}} - E_{\text{on}}(t) \quad t \geq 0. \tag{5}$$

Equation (5) shows that a step-on electric field of a dipole source can be transformed into a step-off electric field by subtracting it from the DC field and *vice versa* (Weidelt, 2000). Note that this relationship is theoretically efficient, but has practical implications as it requires sufficiently long acquisition times to guarantee adequate measurements of E_{DC}.

The inline step-on and step-off electric fields at an offset of 300 m over a homogeneous subsurface of 1 Ωm are displayed in Fig. 1(c–e) for land-based, deep marine (water depth: 5000 m) and shallow marine (water depth: 50 m) environments, respectively. Offsets on the order of hundreds of metres are typically used in marine time-domain controlled source electromagnetic (TD-CSEM) surveys targeting shallow resistive structures in the seafloor (e.g. Schwalenberg *et al.*, 2010). Note that we use the term subsurface to describe the volume of Earth beneath the air/ground or sea/seafloor interface.

Figure 1 shows that the step-on and step-off electric field responses differ between land- and marine-based acquisitions. A land-based step-on transient measured at the surface of a homogeneous half-space is classified into three regions: (i) an early-time voltage where the field is nearly constant and equals $0.5 \times E_{\text{DC}}$, (ii) an intermediate region where the electric field is changing and (iii) a late-time region where the field has reached its steady state (E_{DC}) (Caldwell and Bibby, 1998). In comparison, the land-based step-off data measured over a homogeneous subsurface have the same initial amplitude to the step-on field at early times. As time progresses, the step-off field decays depending on the resistivity of the lower half-space.

When submerged in conductive seawater (0.33 Ωm) (Fig. 1d,e, respectively), the early-time voltages ($t < 10^{-3}$ seconds) of the step-on field equal zero. From (5) it follows that the step-off field must equal E_{DC}. Edwards (2005) states that the time at which this zero-voltage changes depends on the resistivity of the surrounding environment, where a more resistive seafloor will entail amplitude changes at earlier times. One unique feature in marine TD-CSEM acquisition is that early times of the step-off data and late times of step-on data equal E_{DC}. This is not observed on land where an immediate spreading of the signal along the air–ground interface is observed after the transmitter current is turned on or off.
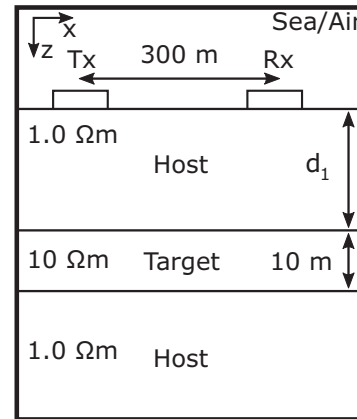

Figure 2 A three-layer Earth model where a 10 m thick layer of 10 Ωm is embedded in a host rock of 1 Ωm at depth d_1 beneath the surface. Transmitter and receiver dipoles are located at the interface between sea/air and subsurface with an offset of 300 m.

TARGET DETECTABILITY ANALYSIS

We use a 1D resistivity model that has a resistive layer of 10 Ωm and 10 m thickness buried in a conductive host rock (1 Ωm) at depth d_1 to illustrate signal characteristics of step-on and step-off electric field data (Fig. 2). Response curves are computed for variable target depths on land, in the deep marine environment and in the shallow marine environment. Figure 3 displays the step-on (green) and step-off (blue) source-normalized electric field transients for a variable target depth ranging between 30 and 100 m. The land-based acquisition is illustrated in Fig. 3(a), the deep marine acquisition in Fig. 3(b) and the shallow marine data in Fig. 3(c). The source and receivers are located on the interface between the air and Earth for the land case and on the seafloor in the marine cases. Figure 3(d–f) shows the corresponding target detectability defined after Goldman *et al.* (2015), also referred to as normalized response curves that are calculated as

$$\text{Detectability} = E_{\text{Target}}/E_{\text{Host}}. \tag{6}$$

Figure 3(a) illustrates that step-on signals on land (green curves) behave similarly to the homogeneous half-space model when a target layer is introduced at a variable depth. During the very early times ($t < 10^{-3}$ seconds), initial amplitudes of the step-on electric field equal

$$E_{\text{ini}} = (\rho_1 \text{Idl})/(2\pi r^3) \tag{7}$$

and depend only on offset (r), transmitter moment (Idl) and resistivity of the uppermost layer ρ_1 (Kaufman and Keller, 1983). Hence, the amplitudes for $t < 10^{-3}$ seconds are equivalent to the half-space response, which equals half the direct current
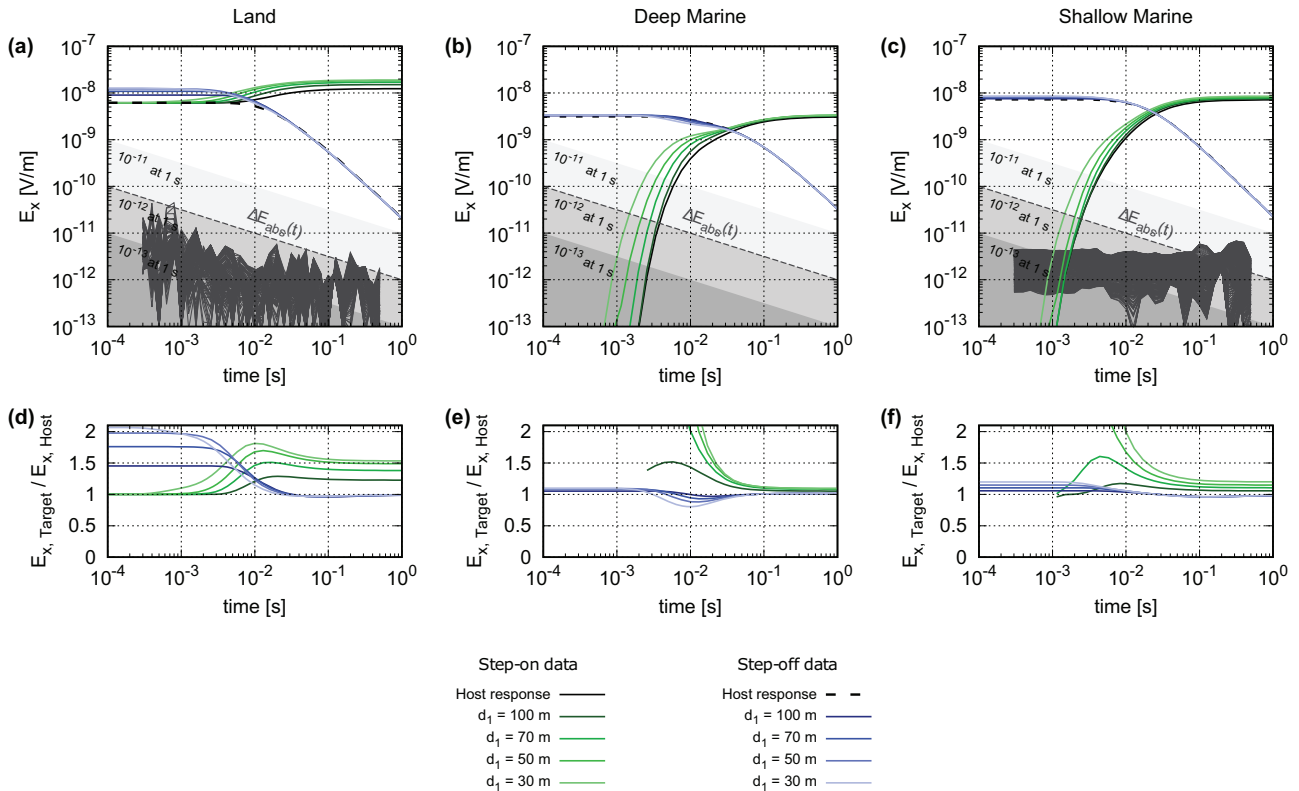
Figure 3 Inline electric field data for (a) land-based, (b) deep marine and (c) shallow marine acquisition using the three-layer subsurface resistivity model presented in Fig. 2. Step-on and step-off electric fields are, respectively, plotted by different shades of green and blue depending on the depth of the resistive target layer. Measured noise data are displayed for reference using thin grey lines, whereas different theoretical time-dependent noise floors are displayed by the different shades of grey in the background. The dashed-grey line represents the time-dependent noise floor (ΔE_{abs}) that is used in the sensitivity and inverse modelling study. Panels (d–f) show normalized response curves for the land-based, deep marine and shallow marine scenario presented in the top panel, respectively. The curves in panels (d–f) are truncated at 2 for better representation of the detectability. Note that the normalized response curves for the marine step-on data increases exponentially until the host-rock response reaches numerical noise. Therefore, we neglect all step-on data for $t < 10^{-3}$ seconds.

(DC) value and is independent of the buried resistive target in the subsurface. This generalization holds for the specific transmitter–receiver separation and sufficiently large depths and low resistivities of the target but may need adjustments to earlier times if violated (i.e. shallower target or more resistive target). As time progresses ($10^{-3} \leq t \leq 10^{-1}$ seconds), field amplitudes of the step-on signal increase at times dictated by the burial depth of the resistive target. At late times (approximately $t > 10^{-1}$ seconds), E_{DC} is reached with the highest amplitudes observed for the shallowest target. The normalized response curves of all target depth variations deviate from unity at $t > 10^{-3}$ seconds, implying a sufficiently high detectability to accurately quantify the depth of the resistive layer in a noise-free environment (Fig. 3d).

The step-off electric fields on land (Fig. 3a, blue curves) subtly depend on the burial depth of the resistive target at early times ($t < 10^{-3}$ seconds) causing an observable difference to the half-space response (dashed black line). As time progresses, the differences diminish and responses cannot be distinguished from the half-space solution at $t > 3 \times 10^{-2}$ seconds. Hence, the target depth information is mainly contained in the early time data of the step-off signal and vanishes as time progresses.

In a deep marine environment (Fig. 3b), the step-on electric fields have an initial amplitude of zero (approximately $t < 10^{-3}$ seconds) and start to increase as the electromagnetic field diffuses through the seafloor. Following Edwards (2005), the time at which the amplitudes change from their zero state depends on the seafloor resistivity and occurs at earlier times for shallower burial depths. As no initial voltage is superimposed on the step-on data, all electric fields show an exceptionally high detectability, exceeding the detectability

of land-based data by several orders of magnitude (Fig. 3e, green lines). In turn, step-off electric fields in the deep marine environment exhibit inferior detectability compared to land-based acquisition. The early-time amplitude that contributes largely to the high detectability on land is equivalent to E_{DC} in the marine environment for all target depths and is therefore relatively insensitive to sub-seafloor resistivity (Swidinksy and Edwards, 2013). At intermediate times, variations in the normalized response curves of the step-off fields are observable (Fig. 3e, blue curves) but remain low compared to step-on data.

In a shallow marine environment (Fig. 3c), step-on electric fields exhibit comparable shapes to the deep-sea setting. In contrast, step-off transients resemble land-based data with a higher detectability observed in the DC voltages at early times. Yet, differences exist between land-based and shallow marine time-domain controlled source electromagnetic (TD-CSEM) acquisition, as early-time amplitudes of the step-off field in a marine setting equal E_{DC} and not $E_{DC} - E_{ini}$. Therefore, early-time marine step-off data have equal detectability to late-time marine step-on data, which is generally lower compared to the land-based acquisition.

Why does the detectability of the inline TD-CSEM electric field change between land and sea? A significant factor is the early-time amplitudes of the step-on data that are observable on land in form of E_{ini} but equal zero within the marine environment. From (7) it is apparent that the early-time voltages ($t < 10^{-3}$ seconds) of the land-based step-on data are identical for all depth variations of the target and depend only on the resistivity of the uppermost subsurface. Contrarily, the DC voltages measured at late times of the step-on data are sensitive to the burial depth of the target layer. From Fig. 3(a), we see that the early-time transients of the step-on and step-off excitation are identical for a homogeneous subsurface but differ in the step-off signal when a resistive target is introduced. Furthermore, when applying (5) we see that early-time voltages of the step-off signal equal $E_{DC} - E_{on}$, where E_{on} is equivalent to the half-space response for $t < 10^{-3}$ seconds. Hence, the early-time amplitudes of the land-based step-off signal contain the subsurface information of E_{DC} minus the background signal of E_{ini}, resulting in an increased detectability of E_{off} compared to E_{DC}.

When translating these land-based observations to the deep and shallow marine environments, the obvious differences in the electric field data are the missing initial voltages of the early-time step-on responses. As (5) also applies within a marine setting, it directly follows that early-time step-off electric field data must equal E_{DC} (Fig. 3b). The conductive

seawater that surrounds transmitter and receiver mitigates an immediate signal spreading after the current switch. As a result, the initial amplitude increase of a marine step-on signal arrives at times that are dictated by the more resistive seafloor and contains the anomalous contribution from the shallow resistive layer (Weidelt, 2007). In contrast, marine step-off data contain the same anomalous contribution caused by the target layer but are superimposed by a much larger DC field at these times. Swidinsky and Edwards (2013) show that the DC field has limited sensitivity towards seafloor resistivity structure and, therefore, a masking effect is observed in the marine step-off data. This is purely a consequence of the high-amplitude and low-sensitivity DC voltage that superimposes the low-amplitude and high-sensitivity inductive currents at early times of step-off data.

Since measured data are superimposed by natural and anthropogenic noise sources, detectability analyses are often limited in significance due to the following aspects. (i) Using normalized response curves to evaluate TD-CSEM signals does not consider noise, which is one of the driving factors in geophysical inversion. (ii) To image the subsurface using linearized inverse modelling, sensitivity is not defined by the ratio of signals with and without a target layer but rather evaluated for small perturbations of each model parameter. Hence, a high detectability does not imply a high sensitivity for specific model parameters, as parameter perturbations will have much smaller effects on the data. As a result, sensitivity may either be masked by the corresponding data error or exhibit intercorrelations between multiple model parameters; neither factor is considered when analysing normalized response curves.

ELECTROMAGNETIC NOISE

Following the noise considerations of Connell and Key (2013) for controlled source electromagnetic (CSEM) data, the absolute ambient electric field noise $\Delta E_{abs}(t)$ can be defined as

$$\Delta E_{abs}(t) = \Delta E_n(t) / \left(Idl\sqrt{N} \right), \tag{8}$$

where $\Delta E_n(t)$ is a time dependent factor in volt per metre, Idl the source moment of the horizontal electrical dipole (HED) in Am and N represents the number of stacked measurements for the final transient. Note that noise decrease proportional to $\sqrt{N}$ is only valid for white Gaussian noise (Munkholm and Auken, 1996). For the source-normalized synthetic data shown in Fig. 3 and the studies presented hereinafter, a source moment of 1 kAm (100 m source length with 10 A current) is used. From (8), it is apparent that the ambient noise can be reduced through a combination of higher source moments

or an increased number of repeated measurements used for stacking. For the following consideration, we neglect error weighting due to repeated stacks ($N = 1$). Moreover, it should be mentioned that $E_n(t)$ contains noise contributions arising from both natural and cultural sources, as well as instrumental noise from system electronics and electrodes (Connell and Key, 2013). We restrain from quantifying different time-dependent noise contributions as these do not affect the results which follow.

Repeated noise measurements from a single site acquired on land and in a shallow marine environment (water depth <50 m) recorded by the same device (KMS820 acquisition unit – KMS Technologies) are displayed in Fig. 3(a,c) by thin grey lines. In both cases, the 50 Hz (and odd harmonics) power grid contributions were filtered, and data were levelled so that the mean voltage of each period equals zero. Subsequently, the recorded 10 kHz data are log-gated following the processing of Munkholm and Auken (1996). Note that the individual noise measurements are not stacked to better exemplify the nature of the background noise for land and shallow marine environments. The presented noise measurements were conducted in different countries; land-based noise measurements are from Cuxhaven, Germany; the marine noise data were measured 4 km offshore Bat Yam, Israel.

For land-based acquisition displayed in Fig. 3(a), a time decay of the absolute noise is observable. This behaviour is consistent with Munkholm and Auken (1996) and should in theory decay with $1/\sqrt{t}$ for Gaussian noise (grey background shading in Fig. 3a,b). For the land-based data, we observe that the decay is slightly more gradual, but remains consistently below the 10^{-12} V/(Am^2) source-normalized noise floor in the time range of interest. The measured noise data in a marine environment behave differently from the land-based case. Here, the $1/\sqrt{t}$ dependency of the noise floor is not observable within the relevant time range, and such non-Gaussian noise is presumably caused by flow noise (motionally induced noise due to water flow around the electrodes as investigated by Djanni, 2016) or cable strumming. But since measured noise data from land and shallow marine environments are predominantly below the absolute noise floor of $\Delta E_{abs}(t) = 10^{-12}/\sqrt{t}$ (illustrated by the thick dashed line in Fig. 3), we define this relationship as adequate for the following 1D sensitivity and inverse modelling studies. We emphasize that the background noise for a specific survey area and measurement system should not be generalized from Fig. 3. The noise data presented here are used as a justification for possible electromagnetic noise encountered in land- and marine-based acquisition. However, noise considerations are survey-specific and should be carefully in-

corporated in a sensitivity analysis prior to inversion as data errors represent one of the driving factors for resolution.

The absolute electric field noise ΔE_{abs} are further superimposed by errors from incorrect survey geometry, synchronization and sensor calibration that have a systematic influence on the measured voltage and cannot be improved by increasing the number of stacks, or using larger transmitter moments (Connell and Key, 2013). Instead, these errors typically scale with the measured voltage and are incorporated by a relative error factor ΔE_{rel}. Studies conducted by Gehrmann *et al.* (2020) show that a quasi-static scaling does not hold true for frequency-domain controlled source electromagnetic (FD-CSEM) applications towed within the water column, where geometrical distortions can be frequency or time dependent. However, such distortions do not concern synthetic data so that a first-order assumption for the total source-normalized error $\Delta E(t)$ can be defined as

$$\Delta E(t) = \Delta E_{rel}E(t) + \Delta E_{abs}(t), \tag{9}$$

where $E(t)$ is the source-normalized electric field for a given transmitter–receiver configuration. In the following, we refer to the studies of Hölz *et al.* (2015) and apply a 1% relative error ($\Delta E_{rel} = 0.01$).

TARGET SENSITIVITY ANALYSIS

Sensitivities of electromagnetic data are defined by the change of the response curve due to a perturbation (typically 10%) of a logarithmically transformed model parameter. Since this does not include any information regarding data errors, the sensitivity matrix ($\mathbf{J}$) is commonly weighted by an error matrix ($\mathbf{W}$), resulting in a dimensionless quantity that makes up the weighted Jacobian matrix ($\mathbf{J}^W$). For electric field data, the weighted Jacobian is defined as

$$W_{ii}J_{ij} = J_{ij}^W = \frac{1}{\Delta E_i}\frac{\partial E_i}{\partial \log(p_j)} = \frac{p_j}{\Delta E_i}\frac{\partial E_i}{\partial p_j}, \tag{10}$$

where $W_{ii} = 1/\Delta E_i$. i refers to the data sample at a specific time and p_j to each model parameter.

The weighted sensitivities of step-on and step-off data are strongly dependent on the characteristics of the data error. Figure 4 illustrates how sensitivity curves for perturbations in target-relevant parameters (i.e. depth: d_1; resistivity: ρ_2; thickness: d_2) change based on relative error weighting in the top row, absolute error weighting from (8) in the second row and total error weighting according to (9) along the third row. Sensitivities are displayed for the land-based case in the left column, the deep marine setting in the centre and for the shal-
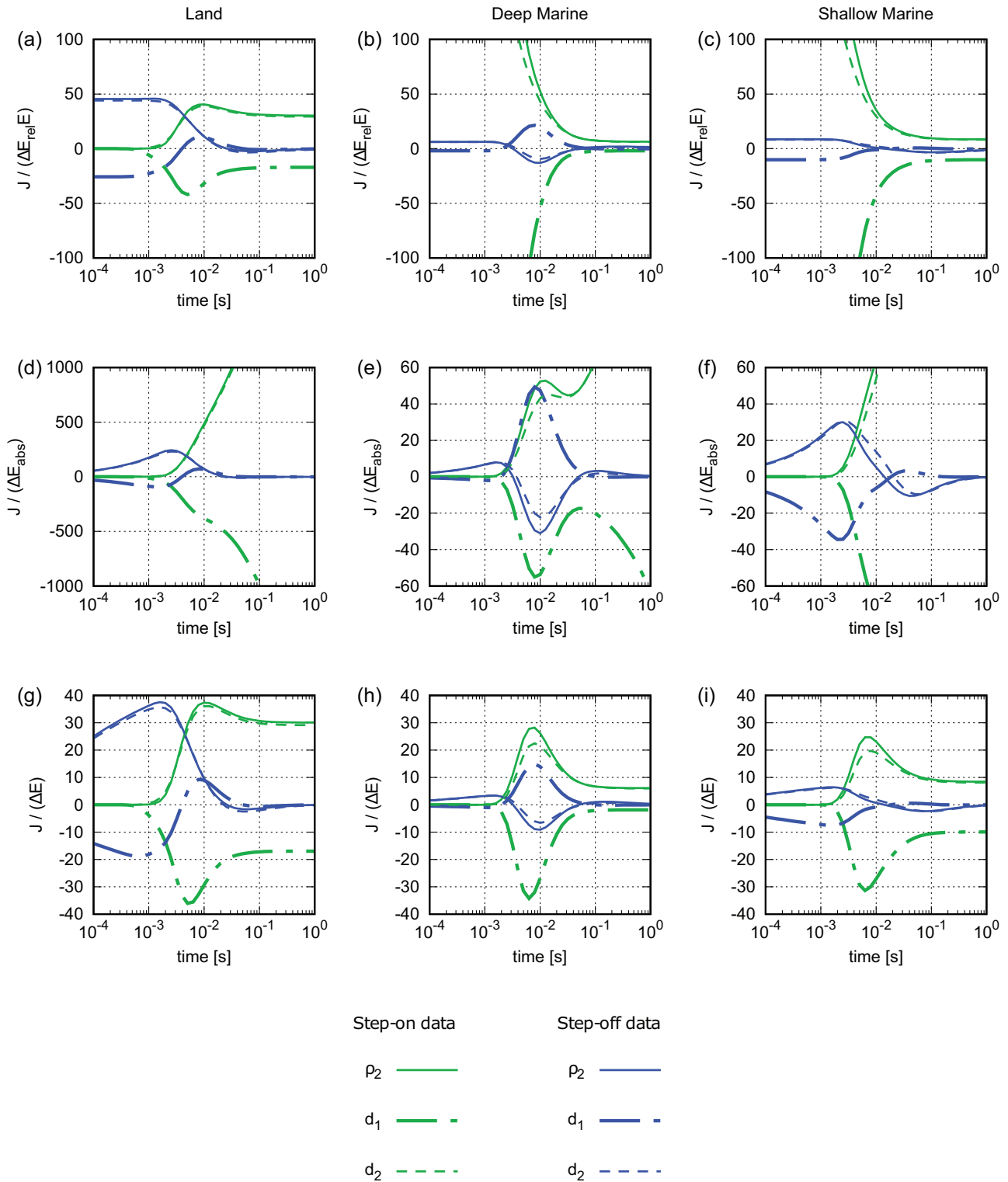
Figure 4 Error-weighted sensitivity curves of (left) land-based, (centre) marine-based and (right) shallow marine-based inline electric field data for the relevant target parameters depth (d_1), thickness (d_2) and resistivity (ρ_2). Step-on and step-off sensitivities are displayed by green and blue lines, respectively. The sensitivity of the target layer resistivity (ρ_2), depth (d_1) and thickness (d_2) are displayed by the different dashed lines. (Top) Relative error weighting, (middle) absolute error weighting and (bottom) total error weighting.

low marine setting along the right column. The green lines refer to the sensitivity of the step-on electric field data, the blue lines to the step-off data. Recall that the unperturbed model has a 10 m thick resistive layer of 10 Ωm embedded in a 1 Ωm host rock at a depth of 50 m.

Weighting the Jacobian with a relative error (Fig. 4a–c) enforces the sensitivity data to resemble the general shape of the normalized response curves shown in Fig. 3(d–f). Note that sensitivity curves of target depth (d_1) have a reversed sign compared to the normalized response curves in Fig. 3 due to the nature of the +10% perturbation, meaning that the target is deeper in the perturbed model and step-on signal amplitudes decrease compared to the unperturbed model. For land-based acquisition, sensitivities of step-off and step-on data are comparable in terms of amplitude. The main sensitivity contributions for target thickness and resistivity are observable at early times in the step-off field and at intermediate to late times in the step-on field. Step-on data are slightly more sensitive to target depth (d_1) compared to step-off data, which exhibit a sign reversal in the sensitivity at approximately 5×10^{-3} seconds (Fig. 4a).

Step-on electric fields acquired in the marine environment exhibit proportionally higher sensitivities compared to step-off fields when weighted by a relative data error, suggesting superior sensitivity (Fig. 4b). This is attributed to the relative error weighting that does not account for an overweighting of sensitivities at times where signal amplitudes are small. In this case, small electric field amplitudes are weighted equivalently to large amplitudes implying a high target sensitivity at early times of the step-on data. But since step-on signals in the marine environment (deep and shallow) are generally orders of magnitude smaller at early times compared to the late-time direct current (DC) field, they are also more susceptible to the superimposed background noise (cf. measured noise data in Fig. 3).

Weighting the sensitivity matrix with an absolute noise floor incorporates the ambient noise and mitigates irregularly high sensitivities caused by small electric field amplitudes (Fig. 4d–f). In turn, absolute error weighting does not consider relative errors that scale linearly with electric field amplitude and, therefore, the sensitivity of the late-time step-on data increase significantly by $\sqrt{t}$ although signal amplitudes are constant. Further differences between relative and absolute error weighting are (i) sensitivities of the early-time step-on data in marine acquisition equal zero since electric field amplitudes are below the absolute noise floor before 2×10^{-3} seconds; (ii) step-off data show a sensitivity decline during early-time windows due to a decrease in signal-to-noise ratios. This re-

sults in sensitivity reduction between 10^{-4} and 10^{-3} seconds for both land- and marine-based acquisition although signal amplitudes are constant within this time window.

Figure 4(g–i) illustrates the sensitivity of time-domain controlled source electromagnetic data weighted by the total error defined in (9). By combining relative and absolute error weighting, characteristics of each are manifested in the sensitivity curves. This error weighting is considered most realistic as measured data typically exhibit both relative and absolute error contributions. The sensitivity curves show an inferior step-off sensitivity towards shallow resistive layers in the deep marine (Fig. 4h) and shallow marine (Fig. 4i) environments. Maximum values of step-on sensitivity exceed step-off sensitivity by a factor of 2 to 3 for all relevant target parameters including depth, thickness and resistivity. These inferior sensitivities observed in the step-off data are due to the superimposing DC contributions at early times that mask the inductive response and only slowly deteriorates. Due to their limited sensitivity to the seafloor resistivity structure, DC voltages suppress the sensitivity of the low-amplitude inductive signal when interpreting step-off data. In comparison to the marine case, step-off data on land are comparable to step-on data in terms of sensitivity since early-time amplitudes are sensitive to variations of the subsurface resistivity structure.

To illustrate sensitivity differences more clearly, the normalized cumulative sensitivity (S_n) defined as (e.g. Martin, 2009)

$$S_n = S_j / \max\left(S_j\right) \;=\; \frac{1}{\max\left(S_j\right)} \frac{1}{A_j} \sum_i^N |J_{ij}^{\mathrm{W}}| \qquad (11)$$

is displayed as a 2D cross-section in Fig. 5. The weighted sensitivity data are computed for the 1D resistivity model displayed in Fig. 2 using a time-domain adaptation of MARE2DEM (Key, 2016) developed by Haroon *et al.* (2018a). In (11), A_j defines the area of each finite element cell, and J_{ij}^{W} is the weighted Jacobian matrix calculated for the unstructured finite-element grid. Normalized cumulative sensitivities are dimensionless quantities that illustrate the sum of error-weighted sensitivities for a specific time range. Here, we consider sensitivities between 10^{-3} and 10^{-1} seconds, where variations in electric field amplitudes are strongest and bias from the static field or early-time voltages is minimized. Figure 5 shows cumulative sensitivities for (left) step-on data and (right) step-off data in (top) land-based, (middle) deep marine and (bottom) shallow marine settings. The colour bar in Fig. 5 highlights regions of high sensitivity by light shading, whereas regions of low sensitivity remain dark.
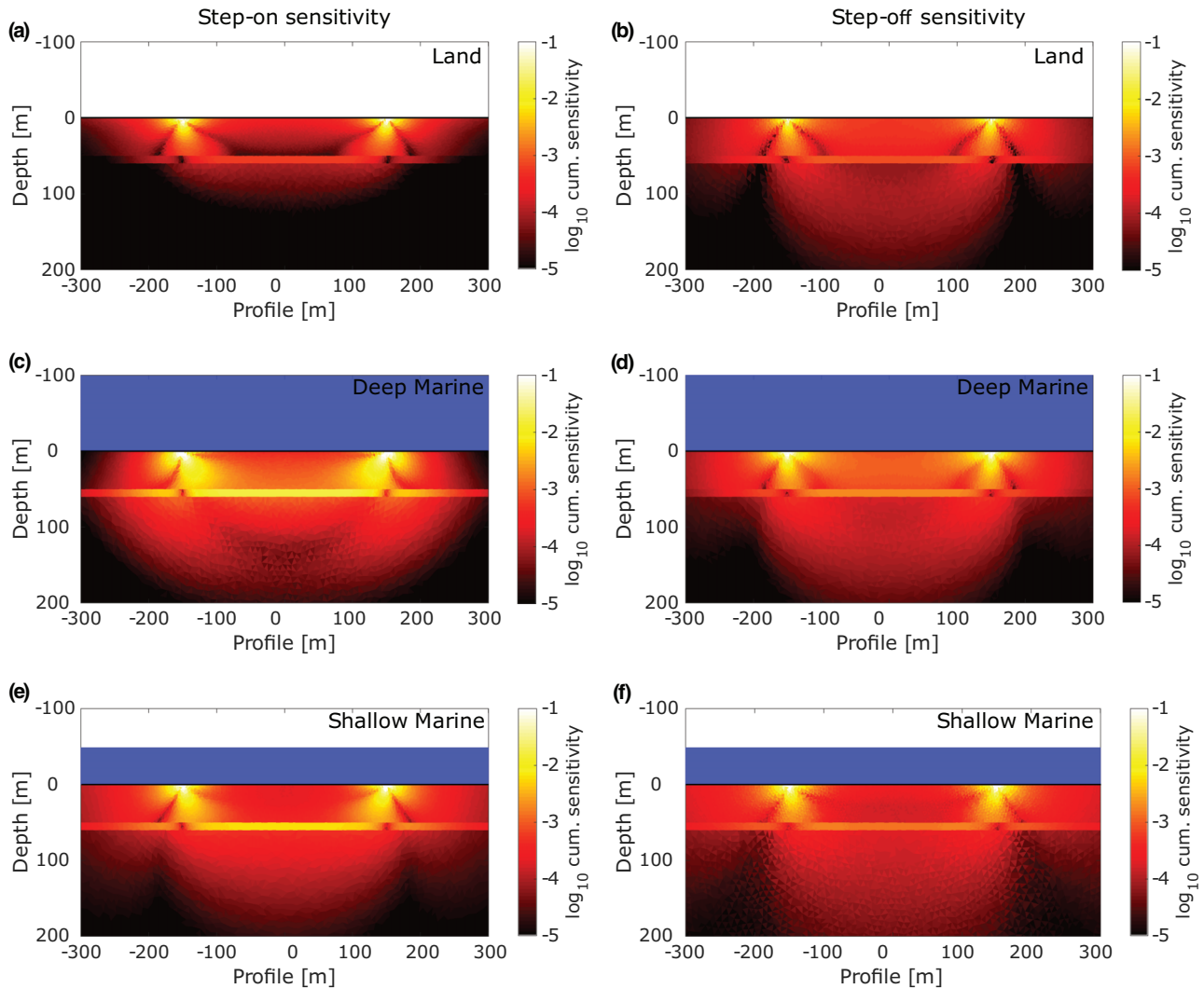
Figure 5 Cumulative sensitivity cross-sections calculated according to equation (11) and plotted for the (top) land-based, (middle) deep marine and (bottom) shallow marine inline electric fields. The step-on and step-off sensitivities are displayed in the left and right panels, respectively. The transmitter and receiver are assumed to be point dipoles located 300 m apart at ±150 m. The interface between the air/sea and subsurface is depicted by a solid black line.

Figure 5(a,b) shows that sensitivities of the resistive target layer are practically equivalent between step-on and step-off data for land-based acquisition. Contrarily, sections located above and below the resistive layer exhibit observable sensitivity differences. On land, the step-on electric field is less sensitive in the section below the resistive layer, which is interpreted as a reduced screening effect following the descriptions of Kaufman and Keller (1983, p. 385). Although the resistivity of the considered target layer is not infinite, a comparable screening effect with decreased significance is observed, where the vortex part of the electromagnetic field becomes insignificant at late times of the step-on signal due to a su-

perimposed relative data error (1% is considered significant). For a step-off field, the vortex character dominates at late times and the field becomes practically horizontal. As a result, resistive layers do not screen regions located at greater depths (Kaufman and Keller, 1983) and imaging these sections is mainly dependent on the magnitude of the absolute noise floor. Sensitivity differences within the overburden between land-based step-on and step-off data are an effect of the considered time window. Here, the considered time window has practically removed E_{ini} defined in (7), and as a result, the step-on data lose cumulative sensitivity towards the overburden.

When submerged in conductive seawater (Fig. 5c–f), sensitivity differences between step-on and step-off fields are mainly observable within the resistive target layer. The bright colouring indicates much higher sensitivity in deep and shallow marine environments when interpreting step-on data. The cumulative step-on sensitivities exceed those of step-off data by nearly one order of magnitude within the resistive target. In turn, sensitivities in sections located above and below the resistive layer appear relatively coherent between step-on and step-off data.

1D INVERSION OF SYNTHETIC DATA

The sensitivity studies presented above demonstrate differences between step-on and step-off fields on land, in the deep sea and within shallow marine environments. They highlight the enhanced sensitivity of step-on electric field data to image shallow resistive targets for deep and shallow marine time-domain controlled source electromagnetic (TD-CSEM) acquisition. However, step-off data are not completely insensitive to shallow resistive targets. The question remains if the higher step-on sensitivity leads to an improved resistivity-depth image through inversion. We perform synthetic inversion studies using an horizontal electrical dipole (HED) source and four inline electric field receivers located at equidistant offsets of 150, 300, 450 and 600 m from the source. Here, multiple receivers at different offsets are applied to (i) mimic a realistic marine TD-CSEM experiment and (ii) enforce a more robust analysis by reducing the ambiguity that would arise from a single source-receiver configuration (e.g. Gehrmann *et al.*, 2016; Schwalenberg *et al.*, 2017).

Before inversion, noise following (9) is added to the synthetic data to simulate realistic noise conditions. Subsequently, the data are inverted using 1D Occam-R1 (Constable *et al.*, 1987) and Levenberg–Marquardt inversion schemes (e.g. Strack, 1992). The resulting models for step-on data, step-off data and a combination of the two data sets (hereinafter referred to as combined inversion) are displayed in Fig. 6. The black model represents the true subsurface resistivity model, the dark-shaded lines the Occam inversions and the light-shaded lines the equivalent Levenberg–Marquardt inversion models using randomly distributed starting models. To analyse a possible interpretation bias due to over-fitting and under-fitting specific receivers, an error-scaled inversion was additionally conducted for land-based and deep marine data where the final model fits all four receivers equally well (Fig. B1). As these error-scaled inversion models are coherent to the displayed models in Fig. 6, we interpret the models ob-

tained from inversion using the original error model defined in (9).

The Occam models shown in Fig. 6 are all fitted to an error-weighted root mean square (RMS) of 1 and converged after seven to nine iterations. Three-layer starting models for the equivalent Levenberg–Marquardt inversions were randomly chosen and all resistivity models displayed in Fig. 6 achieve an error-weighted RMS ≤ 1.

With the exception of the step-off inversion for a shallow marine setting (Fig. 6f), the majority of the obtained resistivity models for both step-on and step-off, and combined inversion indicated the existence of a more resistive layer embedded in a conductive background environment. Overall, target depth, resistivity and thickness are imaged most accurately for the land-based acquisition (Fig. 6, left column) and are more ambiguous when inverting marine data (Fig. 6, centre and right columns).

Resistivity contrasts between the target layer and the background are least pronounced in the marine step-off Occam inversion (Fig. 6e), which is indicative of inferior sensitivity compared to the step-on data (Fig. 6b). This inferior sensitivity is most obvious when analysing the Occam inversion model in a shallow marine environment (Fig. 6f). Here, the step-off data are fit by a homogeneous seafloor model with slightly increased resistivity, whereas the step-on inversion detects the resistive target layer at the correct depth (Fig. 6c). These increased ambiguities within the marine step-off data are further supported by the equivalent Levenberg–Marquardt models that demonstrate a higher variability in the single and combined inversion.

To further illustrate the implications of sensitivity on non-uniqueness of the inversion, target resistivity and thickness are varied between realistic minimum and maximum values. The corresponding error-weighted RMS is shown as a function of ρ_2 and d_2 in Fig. 7. The top row displays the equivalence domain of the step-on data for (a) land, (b) deep marine and (c) shallow marine settings. The bottom row shows the corresponding equivalence domains for step-off data. All images show that target resistivity and thickness are intercorrelated parameters, enabling equivalent data fits for constant resistivity-thickness products if the layer thickness remains ≤ 30 m on land and ≤ 70 m in the marine environment. Overall, step-off data exhibit notable limitations when resolving the resistivity-thickness product compared to step-on data in a marine setting. Equivalent domains (for both shallow and deep marine environments) are notably larger indicating more ambiguity in the target parameters. Figure 7(e) indicates that this ambiguity is largest for step-off data in a deep marine
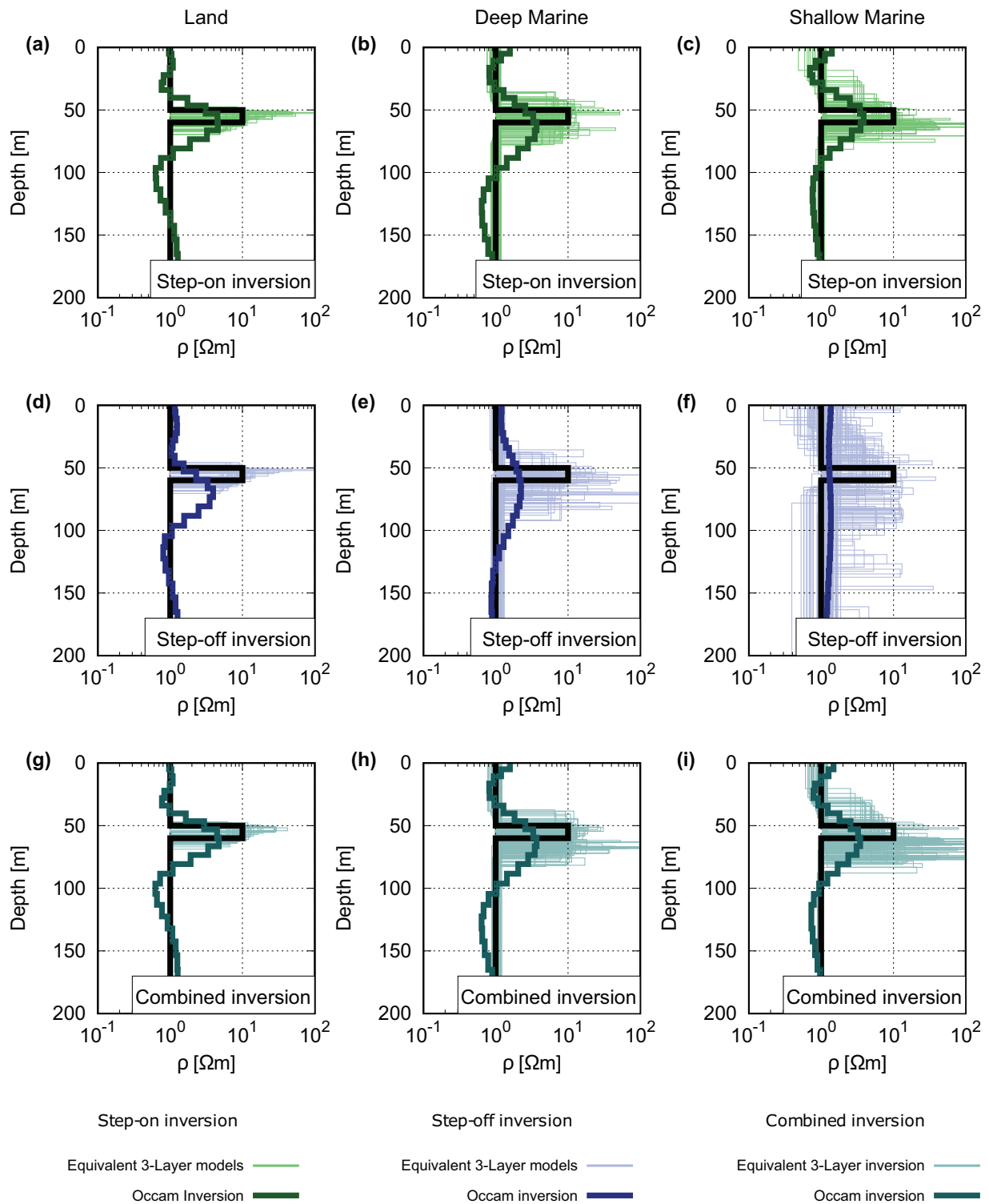
Figure 6 1D inversion models computed using an Occam inversion scheme (dark shading) and three-layer Levenberg–Marquardt inversion scheme for randomly distributed three-layer starting models (light shading). The final inversion models for (left) land, (centre) deep marine and (right) shallow marine are displayed for (top) step-on data, (middle) step-off data and (bottom) a combined inversion approach using both step-on and step-off data. The true model is displayed in each panel by a black line. All Occam inversion models are fitted with an error-weighted RMS = 1, the equivalent Levenberg–Marquardt inversion models are fitted with an RMS ≤ 1.
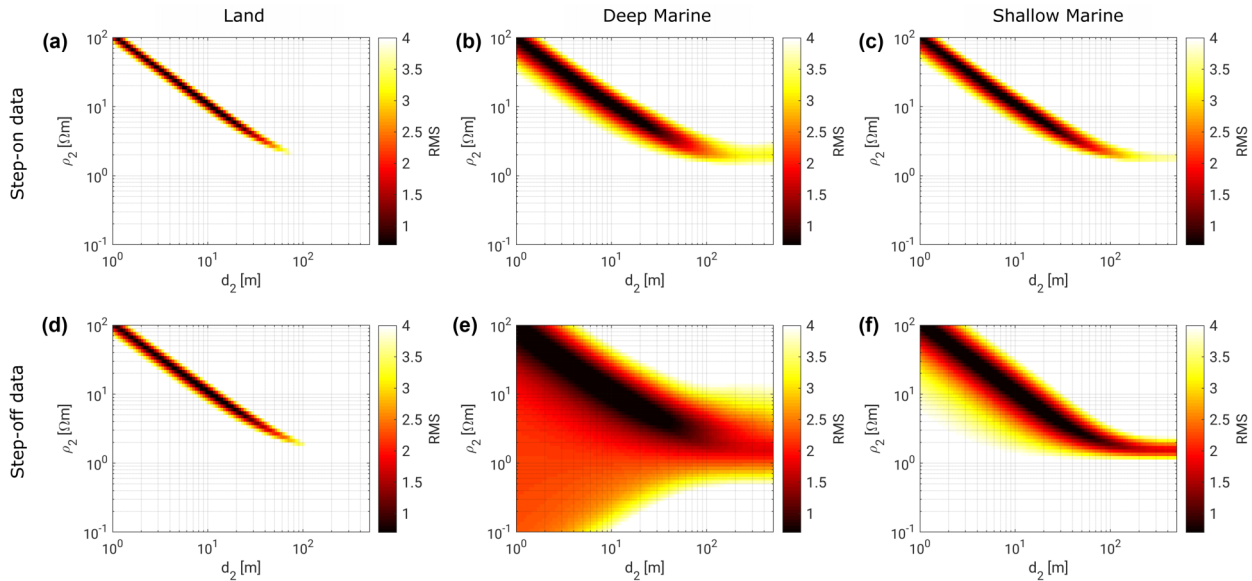
Figure 7 Equivalence domain modelling study of the target layer resistivity (ρ_2) and thickness (d_2) for (left) land, (centre) deep marine and (right) shallow marine environments. The step-on data is displayed on the top, the step-off data along the bottom panels, respectively. The colour scale is chosen so that black colours are considered equivalent within an error-weighted RMS ≤ 1, red colours (RMS ≤ 2) represent parameter combinations with inferior fitting and light/white colours represent parameter combinations that do not fit the data.

environment. However, inter-correlations to other model parameters are not considered here and Fig. 6(f) shows that a shallow marine TD-CSEM acquisition is most affected by its inferior sensitivity.

The sensitivity, inversion and equivalence studies shown in Figs. 5–7 confirm an inferior sensitivity in the marine step-off electric field data when exploring shallow resistive targets in the sub-seafloor. This sensitivity decrease is notable for simple three-layer models, but is even more pronounced when the resistivity-depth structure of the seafloor is more complex. To illustrate this, a final inversion study shows a five-layer resistivity model, where an additional resistive layer of 30 Ωm is introduced at a depth of 100 m beneath the subsurface with a thickness of 50 m (black lines in Fig. 8).

For the inversion of the synthetic five-layer model data, the noise model of (9) is applied for four receivers located at offsets of 150, 300, 450 and 600 m. Figure 8 shows the resulting Occam-R1 and Levenberg–Marquardt inversion models that all achieve an error-weighted RMS = 1 and RMS ≤ 1, respectively. The colour scheme corresponds to Fig. 6.

The left column of Fig. 8 displays the inversion models for land-based acquisition. Here, both step-on and step-off data are able to detect both the shallow and deep resistive layer (Fig. 8a,d, respectively). Resistivity and thickness of the two resistive layers are equally well determined. The equivalent models indicate that the step-on data (Fig. 8a) are superior

in resolving the resistivity of the overburden (ρ_1) due to the defined amplitude of E_{ini}, which is only dependent on the resistivity of the uppermost metres of the subsurface. In turn, the equivalent step-off models indicate superior resolution for the lower terminating half-space. A combined inversion of step-on and step-off data on land (Fig. 8e) includes the resolution characteristics of both data sets. The overburden in the combined inversion is well resolved due to the information content of the step-on data, whereas the lower terminating half-space is well resolved through the step-off data. Additionally, the ambiguities of the combined inversion models for land-based acquisition are further reduced through the increased amount of data in the inversion process (Vozoff and Jupp, 1975). If feasible, a combined inversion of step-on and step-off data is advisable for land-based TD-CSEM applications.

In deep and shallow marine environments, step-on data are more efficient in deriving the true resistivity structure of the subsurface (Fig. 8, centre and right columns). Both step-on and step-off data image the deeper (thicker) resistive layer, but only step-on data can resolve the upper resistive layer. For both data sets the equivalent models express a high ambiguity that is more severe in the step-off inversion. A combined inversion of marine step-on and step-off data shows no significant improvement compared to the single step-on inversion. Thus, we expect that a combined inversion approach for marine data increases non-uniqueness as over-fitted step-off data
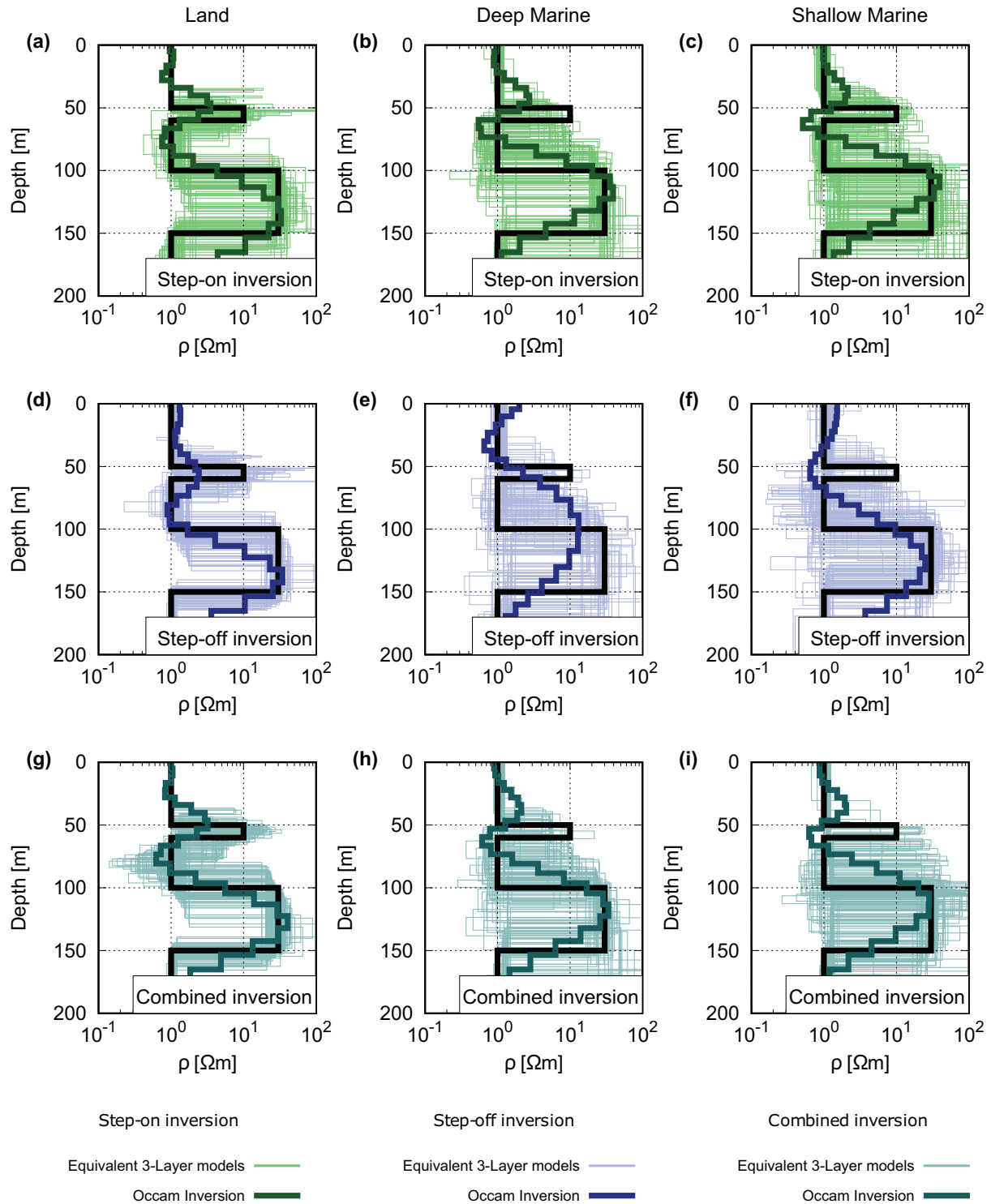
Figure 8 1D inversion models computed using an Occam inversion scheme (dark shading) and five-layer Levenberg–Marquardt inversion scheme for a randomly distributed five-layer starting models (light shading). The final inversion models for (left) land, (centre) deep marine and (right) shallow marine are displayed for (top) step-on data, (middle) step-off data and (bottom) a combined inversion approach using both step-on and step-off data. The true model is displayed in each panel by a black line. All Occam inversion models are fit with an error-weighted RMS = 1, the equivalent Levenberg–Marquardt inversion models are fit with an RMS ≤ 1.

will enforce quicker convergence. However, this assumption is not clearly confirmed by analysis of the equivalent models in Fig. 8(c,i). Still, the analysis indicates that a combined inversion approach does not enhance model parameter resolution for an isotropic marine environment.

DISCUSSION

Due to the preferable step characteristics of a switch-off current function in modern instrumentation, step-off data are widely interpreted in time-domain controlled source electromagnetic (TD-CSEM) experiments. Contrarily, step-on data are often neglected in the interpretation due to non-linear signal distortions caused by the transmitter, which are challenging to account for in processing and inversion. Here, we demonstrate that limiting the interpretation to step-off data prevents TD-CSEM from reaching its maximum potential, particularly when detecting shallow resistive bodies in the marine environment. When submerged in conductive seawater, TD-CSEM data exhibit a notable decrease in step-off sensitivity compared to step-on data. A resistive layer embedded in a conductive seafloor is imaged more precisely using step-on data, especially when resistivity structures are more complex than three-layer models. As a result, the use of step-off data in a single or combined inversion approach appears to be redundant in an isotropic marine environment, as non-uniqueness is increased and resistivity models are more susceptible to misinterpretation. Contrarily, a combined inversion approach on land improves the overall resolution to all subsurface model parameters. Resolution characteristics of both signals are manifested in the best-fit inversion model.

Most continental shelf sedimentary formations are known to exhibit vertically transverse isotropic electrical resistivity (Ramananjaona *et al.*, 2011). Here, we restrict the analysis to isotropic resistivity models to focus on the differences observed between step-on and step-off sensitivities. These demonstrated sensitivity differences are not limited to isotropic resistivity models.

Theoretically, the proposition of only using step-on data in marine TD-CSEM acquisition is easy to recommend. Yet practically, removing non-linear distortions in step-on current functions poses technical challenges that might not find a trivial solution. Hence, measured marine step-on data can contain distortions that prevent an analysis or introduce bias, especially for the shorter offset receivers. In this case, an alternative strategy is imaginable. Transforming the measured step-off data into step-on data using (5) as shown by Mörbe *et al.* (2020) is feasible. However, it is worth clarifying that

the data quality of such derived step-on transient will be inferior due to error propagation. Additionally, the requirement of sufficiently long acquisition times to obtain stable direct current (DC) plateaus can further jeopardize TD-CSEM survey efficiency. This is particularly critical in marine applications where the high cost of ship time is a critical (limiting) factor.

This study focuses on inline electric fields as these are commonly applied in the marine environment to detect shallow resistive structures such as offshore freshened groundwater or gas hydrates. The basic principles presented here also apply to other transmitter–receiver geometries. However, in these cases the implications of possible masking due to superimposed DC amplitudes should be investigated closely. This can be of interest for broadside electric fields, which exhibit a sign reversal in step-off data within the marine environment (e.g. Lippert and Tezkan, 2020). We suggest a thorough analysis of the most effective current function and survey geometry prior to data acquisition.

CONCLUSION

We compare the sensitivity of inline step-on and step-off time-domain controlled source electromagnetic (TD-CSEM) electric field data towards a shallow resistive layer embedded in a more conductive host rock on land and in deep/shallow marine environments. Marine data indicate significantly higher detectability towards shallow resistive layers in the step-on signals compared to step-off signals. By defining realistic data errors for land-based, deep marine and shallow marine TD-CSEM acquisition, we are able to demonstrate that this detectability increase is also observed in the sensitivity, which has implications on geophysical inversion and geological inference. Overall, the inferior sensitivities observed in marine step-off data are explained by the early-time step-off amplitudes, which are sensitive to subsurface resistivity variations on land, but insensitive to resistivity variations in the marine environment. Accordingly, this steady-state response masks the inductive response of the electromagnetic step-off field in the marine environment, substantially reducing sensitivity. In contrast, the step-on signal registered by a marine receiver measures the inductive field component prior to the signal arrival of the steady-state response and contains information about the more resistive seafloor structure. Therefore, the masking effect of the steady-state signal is less significant, resulting in significantly higher sensitivity in comparison.

Synthetic 1D inverse modelling studies indicate that both step-on and step-off electric field data can be used to detect a shallow resistive layer embedded in a conductive host rock.

However, step-off data have inferior sensitivity to these shallow resistive layers in a marine environment, which increases ambiguity of the inversion. Moreover, this inferior sensitivity is further magnified when the resistivity-depth structure of the seafloor is more complex than a three-layer model. Only inversion models that include step-on data can accurately discriminate between two resistive layers embedded in the seafloor at different depths.

DATA AVAILABILITY STATEMENT

Data sharing is not applicable to this paper as no new data were created or analysed in this study.

ORCID

Amir Haroon https://orcid.org/0000-0001-5138-6730
Sebastian Hölz https://orcid.org/0000-0003-2839-9394
Marion Jegen https://orcid.org/0000-0001-6307-8428

REFERENCES

Andreis, D. and MacGregor, L. (2007) Time-domain versus frequency-domain CSEM in shallow water. *SEG Technical Program Expanded Abstracts*. Tulsa, OK: SEG. p. 3124.

Attias, E., Sherman, D., Ismail, K. and Constable, S. (2019) Controlled-source electromagnetic imaging of submarine groundwater reservoirs offshore the island of Hawai'i. Paper H53I-1883 presented at AGU Fall Meeting 2019, San Francisco, USA.

Attias, E., Weitemeyer, K., Hölz, S., Naif, S., Minshull, T.A., Best, A.I. *et al*. (2018) High-resolution resistivity imaging of marine gas hydrate structures by combined inversion of CSEM towed and ocean-bottom receiver data. *Geophysical Journal International*, 214(3), 1701–1714.

Cairns, G. (1997) Development of a short-baseline transient EM Marine System and its application in the study of the TAG hydrothermal mound. PhD Thesis, University of Toronto, Toronto, ON.

Caldwell, G. T. and Bibby, H.M. (1998) The instantaneous apparent resistivity tensor: a visualization scheme for LOTEM electric field measurements. *Geophysical Journal International*, 135(3), 817–834.

Chave, A.D. (2017) Estimation of the magnetotelluric response function: the path from robust estimation to a stable maximum likelihood estimator. *Surveys in Geophysics*, 38, 837–867.

Chave, A.D., Everett, M.E. and Mattsson, J. (2017a) On the physics of frequency-domain controlled source electromagnetics in shallow water. 1: transverse anisotropy. *Geophysical Journal International*, 211(2), 1046–1061.

Chave, A.D., Everett, M.E., Mattsson, J., Boon, J. and Midgley, J. (2017b) On the physics of frequency-domain controlled source electromagnetics in shallow water. 1: isotropic conductivity. *Geophysical Journal International*, 208(2), 1026–1042.

Connell, D. (2011) A comparison of *marine time-domain and frequency-domain controlled source electromagnetic methods*. Master Thesis, University of California, Oakland, CA.

Connell, D. and Key, K. (2013) A numerical comparison of time and frequency-domain marine electromagnetic methods for hydrocarbon exploration in shallow water. *Geophysical Prospecting*, 61(1), 187–199.

Constable, S. (2010) Ten years of marine CSEM for hydrocarbon exploration. *Geophysics*, 75(5), A67–A81.

Constable, S.C., Parker, R.L. and Constable, C.G. (1987) Occam's inversion: a practical algorithm for generating smooth models from electromagnetic sounding data. *Geophysics*, 52(3), 289–300.

Djanni, A.L.T. (2016) Identification and quantification of nose sources in marine towed active electromagnetic data. PhD Thesis, The University of Edinburgh, Edinburgh.

Du, Z. and Key, K. (2018) Case study: North Sea heavy oil reservoir characterization from integrated analysis of towed-streamer EM and dual-sensor seismic data. *The Leading Edge*, 37(8), 608–615.

Edwards, N. (2005) Marine controlled source electromagnetics: principles, methodologies, future commercial applications. *Survey in Geophysics*, 26, 675–700.

Gehrmann, R.A.S., Haroon, A., McKinley, M., Tcheheumeni, D. and Minshull, T. (2020) Seafloor massive sulphide exploration using deep-towed controlled source electromagnetics: navigational uncertainties. *Geophysical Journal International*, 220, 1215–1227.

Gehrmann, R., North, L.J., Graber, S., Szitkar, F., Petersen, S., Minshull, T.A. *et al*. (2019) Marine mineral exploration with controlled source electromagnetics at the TAG hydrothermal field, 26°N Mid-Atlantic Ridge. *Geophysical Research Letters*, 46, 5808–5816.

Gehrmann, R.A.S., Schwalenberg, K., Riedel, M., Spence, G.D., Spieß, V. and Dosso, S.E. (2016) Bayesian inversion of marine controlled

source electromagnetic data offshore Vancouver Island, Canada. *Geophysical Journal International*, 204, 21–38.

Goldman, M., Mogilatov, V., Haroon, A., Levi, E. and Tezkan, B. (2015) Signal detectability of marine electromagnetic methods in the exploration of resistive targets. *Geophysical Prospecting*, 63(1), 192–210.

Goswani, B.K., Weitemeyer, K.A., Minshull, T.A., Sinha, M.C., Westbrook, G.K. and Marin-Moreno, H. (2016) Resistivity image beneath an area of active methane seeps in the west Svalbard continental slope. *Geophysical Journal International*, 207(2), 1286–1302.

Gustafson, C., Key, K. and Evans, R.L. (2019) Aquifer systems extending far offshore on the U.S. Atlantic margin. *Scientific Reports*, 9, 8709. Available at: https://doi.org/10.1038/s41598-019-44611-7.

Haroon, A. (2016) Development of novel time-domain electromagnetic methods for offshore groundwater studies: a data application from Bat Yam, Israel. Doctoral Thesis, University of Cologne, Cologne. Available at: https://kups.ub.uni-koeln.de/7110/.

Haroon, A., Adrian, J., Bergers, R., Gurk, M., Tezkan, B., Mammadov, A.L. *et al.* (2015) Joint inversion of long-offset and central-loop transient electromagnetic data: application to a mud volcano exploration in Perekishkul. *Azerbaijan*, 63(2), 478–494.

Haroon, A., Hölz, S., Weymer, B., Tezkan, B. and Jegen, M. (2018a) Calculating time-domain controlled source electromagnetic signals with MARE2DEM. *3rd Applied Shallow Marine Geophysics Conference*, Porto, Portugal. Available at: https://doi.org/10.3997/2214-4609.201802663.

Haroon, A., Lippert, K., Mogilatov, V. and Tezkan, B. (2018b) First application of the marine differential electric dipole for groundwater investigations: a case study from Bat Yam, Israel. *Geophysics*, 83(2), B59–B76.

Hölz, S., Swidinsky, A., Sommer, M., Jegen, M. and Bialas, J. (2015) The use of rotational invariants for the interpretation of marine CSEM data with a case study from the North Alex mud volcano, West Nile Delta. *Geophysical Journal International*, 201(1), 224–245.

Hördt, A., Jödicke, H., Strack, K.M., Vozoff, K. and Wolfgram, P.A. (1992) Inversion of long-offset TEM soundings near the borehole Münsterland 1, Germany, and comparison with MT measurements. *Geophysical Journal International*, 108(3), 930–940.

Kaufman, A.A. and Keller, G.V. (1983) *Frequency and Transient Soundings*. Amsterdam: Elsevier.

Keller, G.V., Pritchard, J.I., Jacobsen, J.J. and Harthill, N. (1984) Megasource time-domain electromagnetic sounding methods. *Geophysics*, 49(7), 993–1009.

Key, K. (2016) MARE2DEM: a 2-D inversion code for controlled-source electromagnetic and magnetotelluric data. *Geophysical Journal International*, 207(1), 571–588.

Levi, E., Goldman, M., Tibor, G. and Herut, B. (2018) Delineation of Subsea freshwater extension by marine geoelectromagnetic soundings (SE Mediterranean Sea). *Water Resource Management*, 32(4), 3765–3779.

Lippert, K. and Tezkan, B. (2020) On the exploration of a marine aquifer offshore Israel by long-offset transient electromagnetics. *Geophysical Prospecting*, 68(3), 999–1015.

Martin, R. (2009) Development and application of 2D and 3D transient electromagnetic inverse solutions based on adjoint Green func-

tions: a feasibility study for the spatial reconstruction of conductivity distributions by means of sensitivities. Doctoral Thesis, University of Cologne, Cologne. Available at: https://kups.ub.uni-koeln.de/2821/.

Micallef, A., Mountjoy, J.J., Schwalenberg, K., Jegen, M., Weymer, B.A., Woelz, S. *et al.* (2018) How offshore groundwater shapes the seafloor. *Eos*, 99. Available at: https://doi.org/10.1029/2018EO090691.

Micallef, A., Person, M., Haroon, A., Weymer, B.A., Jegen, M., Schwalenberg, K. *et al.* (2020) 3D characterisation and quantification of an offshore freshened groundwater system in the Canterbury Bight. *Nature Communications*, 11, 1372. Available at: https://doi.org/10.1038/s41467-020-14770-7.

Mörbe, W. (2020) Deep controlled *source electromagnetics for mineral exploration: a multidimensional validation study in time and frequency domain*. Doctoral Thesis, University of Cologne, Cologne. Available at: https://kups.ub.uni-koeln.de/10696/.

Mörbe, W., Yogeshwar, P., Tezkan, B. and Hanstein, T. (2020) Deep exploration using long-offset transient electromagnetics: interpretation of field data in time and frequency domain. *Geophysical Prospecting*. Available at: https://doi.org/10.1111/1365-2478.12957.

Munkholm, M.S. and Auken, E. (1996) Electromagnetic noise contamination on transient electromagnetic soundings in culturally disturbed environments. *Journal of Environmental & Engineering Geophysics*, 1(2), 119–127.

Myer, D., Constable, S. and Key, K. (2011) Broad-band waveforms and robust processing for marine CSEM surveys. *Geophysical Journal International*, 184(2), 689–698.

Ramananjaona, C., MacGregor, L. and Andreis, D. (2011) Sensitivity and inversion of marine electromagnetic data in a vertically anisotropic stratified earth. *Geophysical Prospecting*, 59(2), 341–360.

Schwalenberg, K., Haeckel, M., Poort, J. and Jegen, M. (2010) Evaluation of gas hydrate deposits in an active seep area using marine controlled source electromagnetics: result from Opouawe Bank, Hikurangi Margin, New Zealand. *Marine Geology*, 272(1-4), 79–88.

Schwalenberg, K., Rippe, D., Koch, S. and Scholl, C. (2017) Marine-controlled source electromagnetic study of methane seeps and gas hydrates at Opouawe Bank, Hikurangi Margin, New Zealand. *Journal of Geophysical Research: Solid Earth*, 122(5), 3334–3350.

Schwalenberg, K., Willoughby, E., Mir, R. and Edwards, R.N. (2005) Marine gas hydrate electromagnetic signatures in Cascadia and their correlation with seismic blank zones. *First Break*, 23, 57–64.

Sherman, D. and Constable S.C. (2018) Permafrost extent on the Alaskan Beaufort shelf from surface-towed controlled-source electromagnetic surveys. *Journal of Geophysical Research – Solid Earth*, 123, 7253–7265.

Sherman, D., Kannberg, P. and Constable, S. (2017) Surface towed electromagnetic system for mapping of subsea Arctic permafrost. *Earth Planet Science Letters*, 460, 97–104.

Sommer, M., Hölz, S., Moorkamp, M., Swidinsky, A., Heincke, B., Scholl, C. *et al.* (2013) GPU parallelization of a three dimensional marine CSEM code. *Computers & Geosciences*, 58, 91–99.

Strack, K.M. (1992) *Exploration with Deep Transient Electromagnetics*. Amsterdam: Elsevier.

Swidinsky, A. and Edwards, N. (2013) Transient marine electromagnetic responses of 3D resistive structures: implications for navigation. *Geophysics*, 78(1), 1JF–Z24.

Vozoff, K. and Jupp, D.L.B. (1975) Joint inversion of geophysical data. *Geophysical Journal International*, 42(3), 977–991.

Ward, S.H. and Hohmann, G.H. (1988) Electromagnetic theory for geophysical applications. *Electromagnetic Methods in Applied Geophysics: Theory*, Vol. 1. Tulsa, OK: Society of Exploration Geophysicists. Available at: https://doi.org/10.1190/1.9781560802631.ch4.

Weidelt, P. (2000) Numerical modelling of transient-electromagnetic fields in three-dimensional conductors: a comparative study. Elektromagnetische Tiefenforschung, *Kolloquiumsband zur Tagung*, Altenberg, Germany. pp. 216–230.

Weidelt, P. (2007) Guided waves in marine CSEM. *Geophysical Journal International*, 171(1), 153–176.

Weiss, C.J. (2007) The fallacy of the "shallow-water problem" in marine CSEM exploration. *Geophysics*, 72(6), A93–A97.

Weitemeyer, K.A., Constable, S. and Tréhu, A.M. (2011) A marine electromagnetic survey to detect gas hydrate at Hydrate Ridge, Oregon. *Geophysical Journal International*, 187(1), 45–62.

Yuan, J. and Edwards, R.N. (2000) The assessment of marine gas hydrates through electrical remote sounding: hydrate without BSR? *Geophysical Research Letters*, 27(16), 2397–2400.

APPENDIX A: COMPARISON TO FREQUENCY-DOMAIN ELECTROMAGNETICS

The vast majority of controlled source electromagnetics (CSEM) applications that are conducted in the marine environment are practiced in the frequency domain. Commercial exploration for hydrocarbon reservoirs at several kilometres deep below the seafloor uses frequency-domain CSEM (FD-CSEM) due to its effectiveness. Applications in academia are generally confined to shallower resistive structures associated with gas hydrates or offshore freshened groundwater, and CSEM is used in both time and frequency domains. For completeness, we analyse a frequency-domain response based on the forward modelling studies presented in Fig. 3. The resistivity model is displayed in Fig. 2 and the corresponding transmitter–receiver configuration is consistent with the TD-CSEM study we present in the main body of this paper. Note that this study has only limited significance as FD-CSEM systems are generally not seafloor-based with both transmitter and receivers, use a higher variety of offsets to obtain greater depth information and are generally limited to a narrower frequency bandwidth compared to what is presented here. The aim of this study is to demonstrate that a broadband frequency-domain signal is consistent with a step-on time-domain signal as presented above.

Figure A1 shows the FD-CSEM signal magnitudes for an inline electric field receiver at an offset of 300 m from the source. The computed frequency bandwidth is from 10^4 to 10^{-1} Hz. Although the curves are not completely identical with the TD-CSEM step-on signal, the general shape and detectability of the resistive target are consistent. Therefore, the sensitivity of FD-CSEM to shallow resistive layers will behave similarly to the step-on response, provided that error estimations are consistent between time and frequency domains. Yet, it is important to consider the following aspects when comparing the FD-CSEM to TD-CSEM applications. We purposely omit a thorough comparison between time- and frequency-domain CSEM as numerous studies have previously done this. Please refer to Andreis and MacGregor (2007), Connell (2011), Connell and Key (2013) or Mörbe (2020) for detailed comparisons between TD- and FD-CSEM.

1. FD-CSEM applications generally use a smaller frequency bandwidth compared to Fig. A1. Therefore, depth resolution for a single source and receiver pair is limited and such resolution is commonly achieved by using an array of multiple receivers that are located at different offsets from the towed source. When using very large offsets of several kilometres, FD-CSEM applications are capable of investigating targets at several hundred metres to kilometres depth but may have insufficient resolution for very shallow structures.

2. Marine TD-CSEM applications often use several (few) fixed-offset receivers in a seafloor-based system. Increased depth of investigation is obtained through longer acquisition times and by applying larger source-receiver offsets. As a result, TD-CSEM applications are capable of detecting shallow and deep resistive targets in the seafloor.

3. Since FD-CSEM applications do not require the signal to reach a direct current state, they are much more efficient in terms of surveyed profile kilometres.

4. FD-CSEM systems have been applied in both shallow marine (e.g. Sherman *et al.*, 2017; Du and Key, 2018; Gustafson *et al.*, 2019; Attias *et al.*, 2019) and deep marine (e.g. Constable, 2010) environments. Due to its efficiency, a higher lateral data sampling and presumably higher lateral resolution should be achievable using a FD-CSEM system compared to any TD-CSEM for a predefined time frame. Yet, instances exist where TD-CSEM applications may be more suitable, for example in confined coastal areas where only limited offset variations are feasible. Suitability of any CSEM system (TD or FD) for a specific exploration task is survey-specific and also somewhat subjective (e.g. depending on available acquisition hardware, processing and interpretation software, etc.)
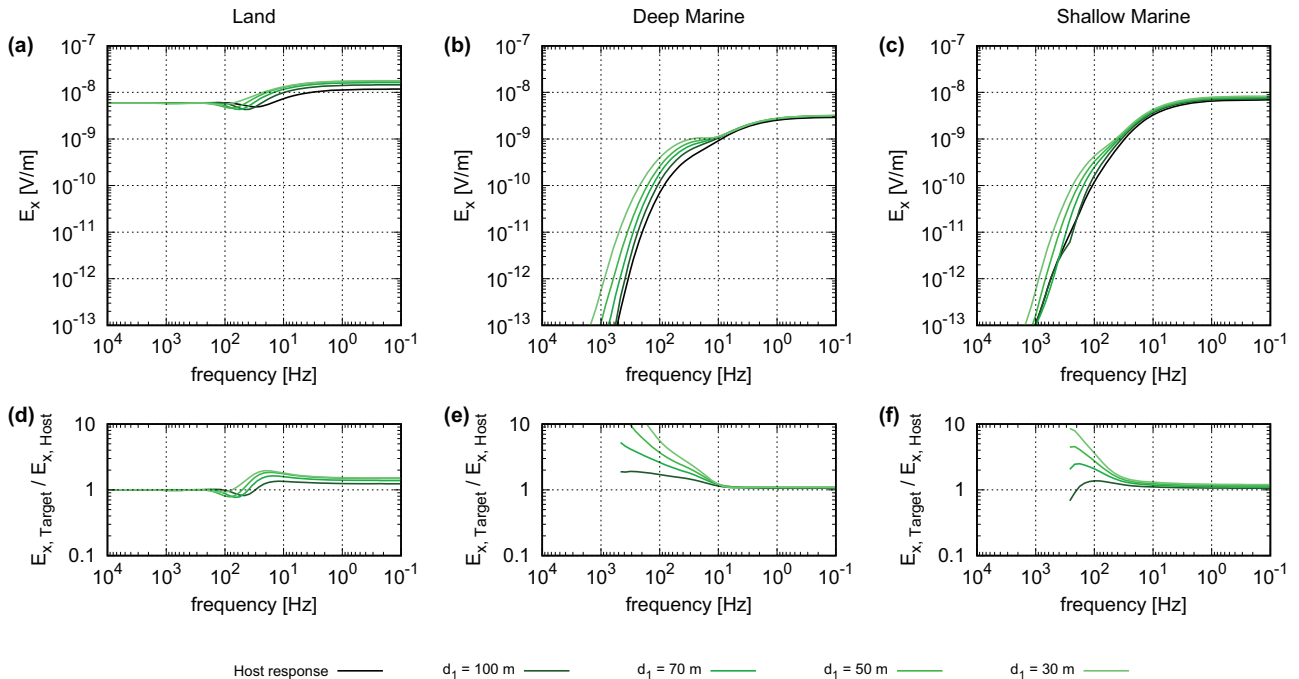
Figure A1 Frequency-domain response for inline electric field data in (a) land-based, (b) deep marine and (c) shallow marine environments using the three-layer subsurface resistivity model presented in Fig. 2. The different shades of green represent varying burial depth of the target layer as indicated in the legend. Panels (d–f) show normalized response curves for the land-based, deep marine and shallow marine scenario, respectively. A normalized response of 1 indicates no detectability towards the target formation at that frequency.

but can be assessed prior to each measuring campaign using forward modelling and error analysis.

APPENDIX B: INVERSION BIAS DUE TO OVER/UNDER-FITTING OF DIFFERENT RECEIVERS

In has been observed that TD-CSEM applications using one source and multiple receivers at various offsets suffer from bias in 1D inversions caused by over-fitting and under-fitting different receivers. Although the overall root mean square (RMS) ≤ 1, the introduced bias can lead to misinterpretation of the obtained resistivity models. An accepted approach to reducing such bias is to conduct multiple hypothesis testing as discussed for magnetotelluric data by Chave (2017). For

CSEM data, Schwalenberg *et al.* (2017) propose a simpler approach based on rescaling the data errors at each receiver so that a resistivity model is obtained where all receivers have an RMS of approximately 1 and the total RMS ≤ 1. We apply the latter approach here. To rule out possible misinterpretation in our inversion studies, we compare inversion results from the original Occam models presented in Fig. 6 to an error-scaled inversion as described above. The inversion models for land-based and marine settings are displayed in Fig. B1. The dark-shaded models are the original inversion models from Fig. 6, and the light-shaded models are the newly computed inversion models. Based on this short analysis, we can conclude that the differences between step-on and step-off resistivity models are not caused by bias of over/under-fitting individual receivers.
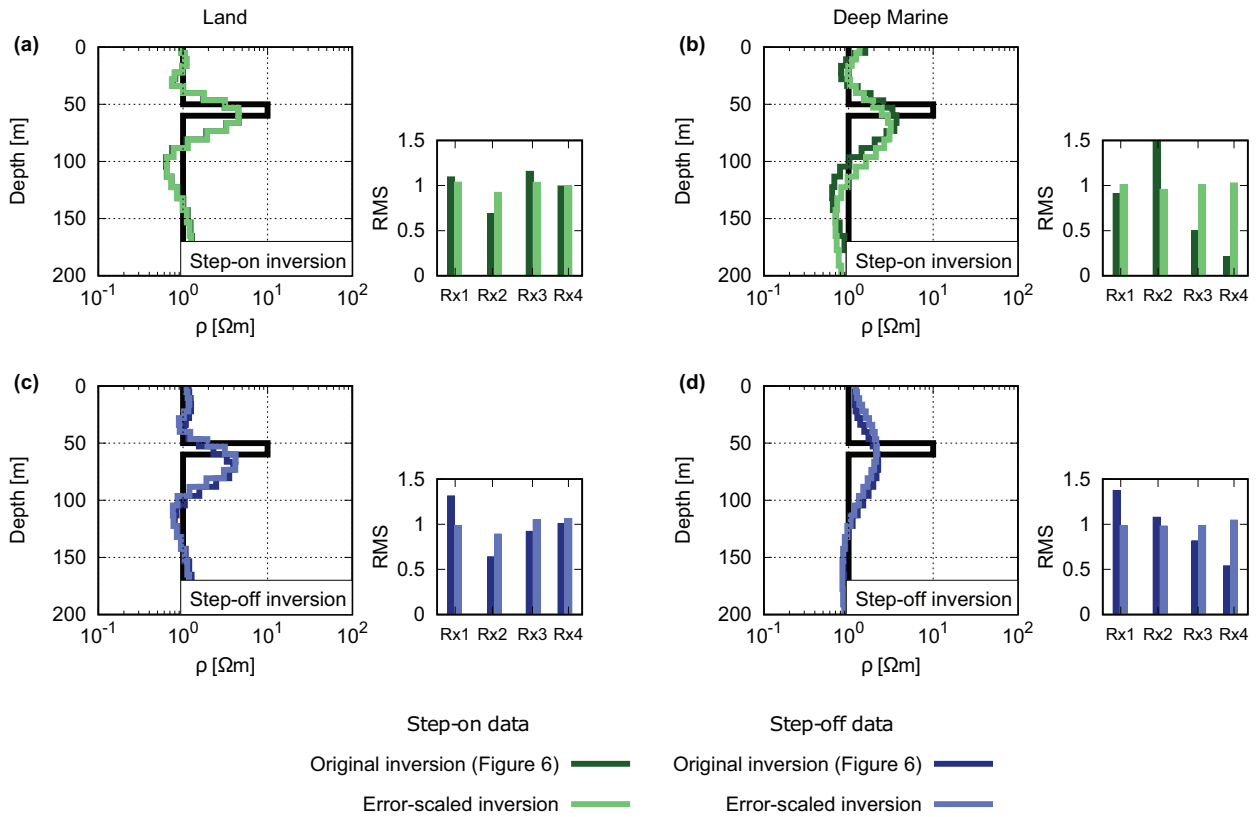
Figure B1 Inversion model comparison for 1D Occam inversion using the original errors using (9) in dark shading and an error-scaled inversion where the errors are scaled so that all receivers are approximately equally well fit in light shading. Panels (a,b) show the respective land and marine case for step-on data; (c,d) show the corresponding inversion results using step-off data. Small sub-panels to the right of each image illustrate the RMS fit at each of the four receivers.